Blood Flow and Oxygen Transport in Descending Branch of Lateral Femoral Circumflex Arteries after Transfemoral Amputation: A Numerical Study

Fei Yan[1,2,3], Wen-Tao Jiang[1,*], Rui-Qi Dong[1,2], Qing-Yuan Wang[1], Yu-Bo Fan[4], Ming Zhang[2,†]

[1]*Laboratory of Biomechanical Engineering, Department of Applied Mechanics, Sichuan University, Chengdu 610065, China*

[2]*Interdisciplinary Division of Biomedical Engineering, The Hong Kong Polytechnic University, Hong Kong, China*

[3]*Institute for Disaster Management and Reconstruction (IDMR), Sichuan University –The Hong Kong Polytechnic University, Chengdu 610065, China*

[4]*School of Biological Science and Medical Engineering, Beihang University, Beijing 100191, China*

Running title: Numerical Simulation of DLFCAs after Amputation

*Corresponding author: Wen-Tao Jiang

E-mail: scubme@aliyun.com

Address: College of Architecture & Environment, Sichuan University, 24 South Section 1, Yihuan Road, Chengdu, China, 610065

Tel.: +86-28-85405140; Fax: +86-28-85405140

†Co-corresponding author: Ming Zhang

E-mail: ming.zhang@polyu.edu.hk

Address: Interdisciplinary Division of Biomedical Engineering, The Hong Kong Polytechnic University, Kowloon, Hong Kong, China

Tel.: +852-27664939; Fax: +852-23342429

ABSTRACT

This study investigates atherosclerotic development in the descending branch of the lateral femoral circumflex artery (DLFCA) after transfemoral amputation and assesses the effects of blood velocity during exercise on the oxygen transport of the residuum DLFCA. Computational fluid dynamics models of DLFCAs coupled with oxygen transport in both the residuum and the sound contralateral limb were established. The profiles for three blood velocity profiles were applied at the inlet of the residuum DLFCA model. The results show that in comparison with the sound limb, blood velocity in the residuum DLFCA was higher, the number of low-wall-shear-stress (WSS) regions was smaller, the Sherwood number for the arterial wall was smaller, and there were more hypoxia zones. An increase in blood velocity in the residuum DLFCA resulted in increases in WSS and the Sherwood number and reductions in the numbers of low-WSS regions and hypoxia zones. The rate of atherosclerosis in the residuum is lower than that of the sound limb in terms of WSS, whereas the rate of atherosclerosis in the sound limb is lower than that of the residuum in terms of hypoxia. Overall, both WSS and oxygen transport need to be considered in order to precisely predict atherosclerosis development in the lower-limb arteries after amputation. In addition, exercise is beneficial for oxygen transport, with an increase in oxygen flux to the arterial wall, and is helpful for the prevention and control of atherosclerosis in the arteries of the residuum.

Keywords**:** Descending branch of lateral femoral circumflex artery (DLFCA), Oxygen transport, Wall shear stress (WSS), Blood velocity, Atherosclerosis

1. Introduction

There were 2.26 million amputees in China in 2006, of which 630,000 needed prostheses [1]. After the Wenchuan and Lushan earthquakes, the number of amputees increased considerably [2].

There are a number of health problems related to wearing prostheses. Friction and pressure result in poor skin micro-circulation and skin problems, such as blisters, edema, and pressure ulcers [3,4]. Damage to deep soft tissue is attributed to high stress in osteotomized bone ends [5]. Moreover, muscle atrophy of the residuum is very common after amputation [6,7]. These issues are disruptive to amputees' daily lives and hinder their clinical rehabilitation, and may even threaten their physical health. As a consequence, numerous studies have been conducted to investigate the mechanism of these problems in order to develop possible interventions for mitigation. For instance, a computational model was employed in the biomechanical analysis at the interface of a residual limb and a prosthetic socket [8]. It was found that there were different distributions of stress and strain in different regions of the residual limb, which could be caused by the biomechanical mechanism of loading transfer. Mak et al. [9] concluded that biomechanical consideration is required in the design of each component in a prosthesis, so as to improve the surface biomechanical state of the residual limb. In addition, it has been demonstrated that the decrease of muscle fibre size is the main contributor to muscle atrophy [10]. The fundamental mechanisms of these problems have not been fully elucidated. Thus, studies on residuum disorders are of great significance in biomechanical research.

The spatial vasculature of the residuum is changed significantly by lower-limb amputation. Limb amputation can directly contribute to a partial loss of the vasculature and gradually narrow the arteries of the residual limb [11-13]. Moreover, residuum muscle atrophy may cause spatial structure changes and lumen reconstruction of the branch vessel after amputation. The pressure in the prosthetic socket causes the extrusion of some vessels (mainly veins) after wearing prostheses. In summary, there are differences between the residuum and a sound contralateral limb in terms of vasculature geometry. A vast amount of research has proven that changes in the vasculature geometry could affect the hemodynamic status and oxygen transport in the arteries [14-18], with some studies employing coupled numerical analysis of the hemodynamic status and oxygen transport in the arteries based on fluid mechanics and mass transfer theories. The hemodynamic status of the arteries could affect the value of the wall shear stress (WSS) [19,20]. Low WSS enhances intimal thickness whereas high WSS inhibits it [21,22]. Low WSS could have further effects on the development of atherosclerosis [23,24]. In addition, high oxygen tension can promote the rate of successful stump healing [25-27], and hypoxia (low oxygen tension) in the residuum facilitates muscle protein degradation via a decrease in muscle protein synthesis, which contributes to muscle atrophy after amputation [28]. Consequently, it is necessary to investigate the hemodynamic status and oxygen transport in the vasculature of the residuum, which is beneficial in evaluating the residuum status. Previous studies on blood flow in the residuum mainly focused on the microcirculation of soft tissue [9,29]. Few investigations have focused on the blood flow and oxygen transport in the residuum arteries after amputation. The objective of this study is to investigate the hemodynamic status and oxygen concentration in the residuum arteries after amputation. Computational simulations of blood flow and oxygen transport in the arteries of the residuum and the sound limb were carried out.

2. Materials and Methods

2.1 Models

Angiographic images of a unilateral transfemoral amputee were acquired utilizing a dual-source computed tomography (CT) system (Siemens Somatom® Definition Flash, Siemens Healthcare Sector, Forchheim, Germany). These images were collected from a 21-year-old female volunteer who had undergone left mid-thigh amputation. There were 717 slices with a thickness of 1 mm in the angiographic images. The field of view was 377×377 mm^2, the image resolution was 512×512 pixels, and the pixel size was 0.736 mm. This study was approved by the Human Subjects Ethics Sub-committee of The Hong Kong Polytechnic University. Informed consent was obtained from all individual participants included in the study.

Muscle atrophy of the residuum sartorius and quadriceps femoris, which is related to disuse atrophy, is most obvious after amputation [7]. The descending branch of the lateral femoral circumflex artery (DLFCA) is the main vessel that supplies nutrition and oxygen for these muscles [30]. The DLFCA is the longest branch with a low rate of atherosclerosis formation [31,32]. Based on the angiographic images, there were changes in the geometry of the residuum DLFCA after amputation. Specifically, the bifurcation of DLFCA in the residual limb was not present, unlike in the sound limb (Fig. 1), and the mean diameter of the vessel in the residuum was smaller than that of the sound limb (Fig. 2(c)). Thus, the possible formation of atherosclerotic plaques in this vessel after amputation was examined. Three-dimensional (3D) models of DLFCAs in both the residuum and the sound contralateral limb (Fig. 1) were reconstructed using Mimics (version 10.0, Materialise, Leuven, Belgium) and Gambit (version 2.3, ANSYS, Inc., USA). Firstly, the initial 3D geometric model was built in Mimics after the boundary of the vessel was segmented manually.

Subsequently, the fit centerline in Mimics was applied for extracting the centerline of the vessel and the diameters of some cross-sections perpendicular to the centerline. Then, circles perpendicular to the centerline were built in Gambit using the diameters and the coordinates of the centerline. Finally, the skin surface in Gambit was employed for reconstructing the vascular wall, and the 3D model was created using the wall surface. The diameters of the vascular model in the sound limb and the residuum at the inlet were 4.143 and 3.244 mm, respectively.

The geometric models were meshed in Gambit (Fig. 2). There were 1,339,507 mixed elements in the vascular model of the sound limb, which consisted of 1,044,127 tetrahedral elements in the interior and 295,380 high-quality wedge elements within the boundary layer. The minimum element size was 4.831139×10^{-14} m^3, and the maximum element size was 2.189661×10^{-12} m^3. 93% of elements had an aspect ratio of 1 to 4, and 93% of elements had a skewness of 0 to 0.4, with no elements exceeding 0.95. In addition, there were 740,426 mixed cells in the model of the residuum, which included 523,352 tetrahedral elements in the interior and 217,074 high-quality wedge elements within the boundary layer. The minimum element size was 2.980852×10^{-14} m^3, and the maximum element size was 1.283296×10^{-12} m^3. 75% of elements had an aspect ratio of 1 to 4, and 95% of elements had a skewness of 0 to 0.4, with no elements exceededing 0.95. More elements were meshed within the boundary layer to increase computational accuracy. In Fluent, grid adaptation was employed to keep results mesh-independent. When the results became mesh-independent, grid refinement was stopped.

2.2 Boundary conditions

Three assumptions were employed in this numerical analysis of blood flow: blood is a homogeneous, incompressible fluid [33]; the walls of vessels are rigid and no-slip [34,35]; and blood flow is steady. Although blood is actually pulsatile [36], studies have proven that the distribution of oxygen content and blood flow can be studied qualitatively under the assumption of steady flow [15,37-39]. Moreover, the elasticity of the arterial wall is supposed to rarely affect the simulation results of blood flow in femoral arteries [40]. Thus, the vascular wall was assumed to be rigid and no-slip. In the simulation of blood flow, the 3D continuity equation and the Navier-Stokes equation were applied.

$$\begin{cases} \dfrac{\partial u_j}{\partial x_j} = 0 \\ \rho \dfrac{\partial (u_j u_i)}{\partial x_j} = -\dfrac{\partial P}{\partial x_i} + \mu \dfrac{\partial}{\partial x_j}\left(\dfrac{\partial u_i}{\partial x_j} + \dfrac{\partial u_j}{\partial x_i}\right) \end{cases} \qquad (i, j = 1,2,3) \qquad (1)$$

where u_i is the velocity vector of blood, and P is the pressure. Moreover, ρ and μ are the density and dynamic viscosity of blood, respectively, where ρ =1050 kg/m^3 [41].

Blood is regarded as a complex non-Newtonian fluid [42-44], and in this study, the Casson model was applied. By utilizing the mathematical expression of a Newtonian fluid in terms of the Casson equation ($\sqrt{\tau} = k_0 + k_1\sqrt{\dot{\gamma}}$), the apparent viscosity of the Casson model can be derived as $\mu = \dfrac{1}{2\sqrt{D}}\left(k_0 + k_1\sqrt{2\sqrt{D}}\right)^2$ [45], where τ and $\dot{\gamma}$ are the shear stress and shear strain, respectively; k_0^2 and k_1^2 are the Casson yield stress and Casson viscosity, respectively; and D is the second invariant of the strain rate tensor. The modified viscosity is applicable for the Casson model.

The pressure at the outlet was set as zero: $P|_{outlet} = 0$. Since exercise contributes to an increase in blood flow velocity [46], it was necessary to investigate the impact of exercise on the oxygen transport in the DLFCA. In order to determine the effect of blood velocity on oxygen transport, the profiles for three blood velocities were applied at the inlet:

$$\begin{cases} V_z\big|_{inlet} = 0.091\ m/s\ (velocityA),\ 0.245\ m/s\ (velocityB),\ 0.321\ m/s\ (velocityC) \\ V_r\big|_{inlet} = 0 \end{cases} \quad (2)$$ [46]

where V_z and V_r are the blood velocities in the axial and radial directions, respectively. r is the radius of the vessel. Moreover, *velocityA* represents the mean blood velocity at rest; *velocityB* represents the mean blood velocity during exercise; and *velocityC* represents the mean blood velocity during steady-state exercise. During steady-state exercise, the energy expenditure is balanced with the energy required to perform the exercise [47].

Oxygen transport of the blood flow is composed of convection and diffusion terms, expressed by the following equation:

$$\left(1+\frac{[Hb]}{\alpha}\frac{dS}{dPO_2}\right)\vec{u}\cdot\nabla PO_2 = \nabla\cdot\left[D_b\left(1+\frac{[Hb]}{\alpha}\frac{D_c}{D_b}\frac{dS}{dPO_2}\right)\nabla PO_2\right] \quad (3)$$

where PO_2 is the oxygen tension in blood flow. The ability of hemoglobin to carry oxygen in blood is expressed by $[Hb]$, and α is the oxygen solubility. D_b and D_c are the diffusion coefficients of free oxygen and oxyhemoglobin, respectively. The ratio of oxyhemoglobin to total hemoglobin, S, is referred to as the saturation function, given by the Hill equation: $S = \frac{PO_2{}^n}{PO_2{}^n + PO_{50}{}^n}$ [48]. These parameters are derived from the literatures (Tab. 1).

At the inlet, the boundary condition of the oxygen tension was set as $PO_2\big|_{inlet} = 80\ mmHg$; the flux of oxygen tension at the outlet was specified as $\frac{\partial PO_2}{\partial n} = 0$; and oxygen tension of the vascular wall was set as $PO_2\big|_{wall} = 60\ mmHg$ [49,50,14].

The commercial computational fluid dynamics (CFD) package Fluent (version 6.3, ANSYS, Inc.), based on the finite volume method, was used to solve the equations of blood flow and oxygen transport; the solver was based on pressure. The user-defined scalar (UDS) in Fluent was used for solving the oxygen transport equation with the user-defined C-like function (UDF). The apparent viscosity of the Casson model was employed in Fluent by compiling the UDF. Moreover, the computational model utilized the 3D single-precision and segregated solver. In the solution controls, the SIMPLEC method was set for pressure-velocity coupling; the solution of pressure applied standard discretization; and the first-order upwind was employed in the discretization of the momentum and oxygen tension. A residual value of 0.0001, which might be enough for complex 3D models, was selected as the absolute convergence criterion for all the variables. The model of the sound limb required 286 iterations to converge. The numbers of iterations for three inlet velocities were 278, 296, and 312 in the model of the residual limb, respectively.

3. Results

3.1 Comparison of DLFCA between the residuum and sound limb

The geometry of residuum vasculature was changed significantly after the amputation. There were remarkable differences in the geometry of DLFCA between the residuum and sound limb based on the angiographic images. The bifurcation of DLFCA in the residuum was not present, unlike in the sound limb (Fig. 1), but may have existed before amputation. The amputation might contribute to the disappearance of the bifurcation. The mean diameter of this vessel in the residuum was 20.8% smaller than that of the sound limb (Fig. 3(c)). As mentioned above, the limb amputation could narrow the arteries of the residuum gradually, and the extrusion of the vessel by the atrophied muscles may cause reduction in the diameter of the vessel.

3.1.1 *Velocity and WSS*

The inlet boundary with *velocityA*, which represents the mean velocity at rest, was applied in the vascular model of the residuum and sound limb. As shown in Figs. 3(a) and 3(b), there were significant differences in the distribution of blood velocity between the residuum and sound limb, which resulted from the changes in the DLFCA of the residuum after amputation. The blood velocity in the residuum was higher than that of the sound limb, as shown in Fig. 3(d). This was due to the diameter of the DLFCA in the residuum being smaller than that of the sound limb.

The WSS of the vessel plays a significant role in the evaluation of vascular diseases. A WSS value smaller than 0.4 Pa is unfavorable for the vessel [22], and may contribute to the development of vascular diseases. The region of the vascular wall whose WSS value is smaller than 0.4 Pa is referred to as a low-WSS region. The number of low-WSS regions in the sound contralateral limb was larger than that in the residuum, as shown in Fig. 4. This might be due to the fact that the bifurcation in the sound limb disturbed blood flow, the blood velocity in the sound limb was lower than that of the residuum, and the recirculation zones, which were caused by the lower blood velocity and bifurcation, resulted in more low-WSS regions in the DLFCA of the sound limb. More specifically, low-WSS regions were observed in the curved region of the vessel near the outlet in the residuum, and near the bifurcation and the outlet of the vascular model in the sound contralateral limb.

3.1.2 *Sherwood number*

Hypoxia (low oxygen tension) occurs in the region of the vascular wall where the Sherwood number is smaller than the Damköhler number [14,51,52]. The Sherwood number, given by the expression ($Sh = k\frac{a}{D}$), is a dimensionless coefficient in the mass transfer process. In the equation,

k denotes the coefficient of mass transfer and is equal to $\frac{-D\frac{\partial PO_2}{\partial n}\big|_w}{PO_2\big|_{inlet} - PO_2\big|_{wall}}$ [15]; a represents the mean diameter of the vessel; and D is defined as the diffusion coefficient of oxygen. The Damköhler number is regarded as a dimensionless wall consumption rate coefficient, expressed as $Da_w = \frac{\dot{Q}Ta}{KDP_b}$ [48], where $\dot{Q}$ is the oxygen consumption rate of arterial tissue; a represents the mean diameter of the vessel; T is the thickness of the arterial wall; K is Henry's law constant; D denotes the diffusion coefficient of oxygen; and the bulk oxygen partial pressure is expressed by P_b. The estimated value of the Damköhler number was 39 for simplification [14]. The post-processing with the UDF in Fluent was applied for calculating the Sherwood number.

As shown in Figs. 5(a) and (b), hypoxia zones were observed near the inlet and in the middle of the residuum DLFCA model, whereas the sound limb had no hypoxia zones. Moreover, the Sherwood number in the arterial wall of the sound contralateral limb was larger than that of the residuum (Fig. 5(c)). The mean oxygen tension in DLFCA of the sound limb was slightly smaller than that of the residuum, as shown in Fig. 5(d).

3.2 Comparison of three inlet velocities in residuum

3.2.1 *Velocity and WSS*

To determine the effects of inlet velocity on blood flow and oxygen transport in the DLFCA of the residuum, the profiles for three blood velocities were applied at the inlet of the vascular model: 0.091 m/s (*velocityA*); 0.245 m/s (*velocityB*); and 0.321 m/s (*velocityC*). When the velocity at the inlet boundary increased, the velocity of blood flow also increased (Fig. 6). For most regions of the vessel, there was no difference in the streamline distribution among the three inlet boundary conditions (Figs. 6(a)-(c)). However, the streamline distribution in the region close to the outlet was disturbed for *velocityB* and *velocityC* (Figs. 6(e) and (f)). Specifically, there was an elongated recirculation zone close to the outlet of the vascular model for these two inlet velocities. In summary, the increment of the velocity at the inlet could contribute to the increase in blood flow velocity, and result in the formation of a recirculation zone in the region near the outlet.

As shown in Fig. 7, a low-WSS region appeared in the vascular model only with *velocityA*. This region was observed in the curved region of the vessel near the outlet. It should be noted that the value of WSS increased, followed by an increment of the blood velocity at the inlet boundary. That is, the increase in the inlet velocity contributes to the increase in WSS, reducing the number of low-WSS regions. Since low WSS can contribute to the formation of atherosclerotic plaque [22], the increment of the inlet velocity in the DLFCA could reduce the risk of atherosclerosis.

3.2.2 *Sherwood number*

For the three velocities at the inlet, the mean Sherwood number with *velocityC* was the largest (Fig. 8(d)). With an increment of the inlet velocity, the Sherwood number in the wall of the vascular model increased, as shown in Fig. 8. As shown in Figs. 8(a) and (b), hypoxia zones were observed near the inlet and in the middle region of the residuum DLFCA model. Thus, the number of hypoxia zones in the residuum DLFCA reduced with the increase in inlet velocity. In summary, the increase in the blood velocity at the inlet of the DLFCA was the main contributor to the decrease in the number of hypoxia zones in the vascular wall, which is beneficial for oxygen transfer in the vessel.

4. Discussion

It was reported that instantaneous WSS obtained with consideration of vessel wall elasticity was only 20% lower than that of the rigid model at peak systole due to the low distensibility of the femoral artery [40]. Also, the distensibility of the DLFCA in the residual limb should be lower than that of the femoral artery. Therefore, the vessel wall elasticity of this branch should have little effect on hemodynamic parameters in numerical analysis. Moreover, researchers usually assume the arterial wall to be rigid in computational models with oxygen transport [15,14]. Under the assumption of a rigid wall, the distribution of oxygen tension in the arterial wall can be investigated qualitatively [17,53], which is helpful for finding hypoxia zones. The key point of the present study was to find hypoxia zones in the vascular wall of the DLFCA, and this assumption is reasonable for this research. In addition, the blood flow was treated as steady. Although blood is actually pulsatile [36], studies have demonstrated that the distribution of oxygen tension can be found using the assumption of steady flow [37-39,54,55].

There were differences in the geometry of the DLFCA between the residuum and sound contralateral limb: the bifurcation of this vessel in the residuum was removed and the diameter of the residuum DLFCA was smaller. This may be due to the fact that limb amputation narrows the vessels of the residuum gradually, and the extrusion of the vessel by the atrophied muscles might contribute to the decrease in diameter. Since the residuum DLFCA is narrowed, the blood velocity in the residuum becomes higher. The number and area of low-WSS regions in the residuum were smaller than those of the sound limb. This might be due to the fact that the bifurcation in the sound limb disturbed blood flow, and the blood velocity in the residuum was higher than that of the sound contralateral limb. Therefore, more recirculation zones, which were caused by lower blood velocity and bifurcation, contributed to more low-WSS regions in the DLFCA of the sound limb. Low WSS enhances intimal thickness whereas high WSS inhibits it [21,22]. Chatzizisis et al. [23] suggested that low WSS could enhance the lipid accumulation in the vascular segment, which would contribute to the formation of atherosclerotic plaque. Some scholars reported that the location of the atherosclerotic plaque coincided with the low-WSS region [24,56]. As a consequence, there is a remarkable correlation between low WSS and atherosclerotic development. CFD models have been employed for the assessment of atherosclerotic development using this low WSS theory [57,58]. The formation of atherosclerotic plaque is unfavorable for the health status of the lower limb. Consequently, in terms of WSS, the rate of atherosclerosis in the residuum should be lower than that of the sound limb after amputation.

Hypoxia is another contributor to the formation of atherosclerotic plaque [52]. Hypoxia contributes to the increase in the permeability of endothelium to macromolecules by damaging the endothelium and enhancing interendothelial cell gaps [59]. It can also influence the permeability of endothelium by up-regulating the amount of vascular endothelial growth factor (VEGF) [51]. With hypoxia, more low-density lipoprotein (LDL) penetrates into the arterial wall through a leaky junction, which is caused by endothelial apoptosis [60]. Consequently, hypoxia causes LDL accumulation in the arterial wall and promotes the formation of atherosclerotic plaque [61].

The Sherwood number is a dimensionless coefficient for the mass transfer process, and can be treated as a criterion for defining the hypoxia zone. In terms of oxygen transport, the Sherwood number in the arterial wall of the residuum was smaller than that of the sound limb, and the number of hypoxia zones in the residuum was greater than that of the sound contralateral limb. The oxygen transport may be hindered in the narrow DLFCA of the residuum, which could result in an increment of the number of hypoxia zones. As a consequence, the rate of atherosclerosis in the sound limb is lower than that of the residuum in terms of hypoxia. In summary, the rate of atherosclerosis in residuum DLFCA is lower than that of the sound limb in terms of WSS, whereas in terms of the Sherwood number, the formation rate of atherosclerotic plaque in the sound limb is lower than that of the residuum. In other words, there was no tendency for the Sherwood number to be smaller than the Damköhler number in the low-WSS regions, which is consistent with the results of a previous study [15]. Liu et al. found that zones with small Sherwood numbers were not consistent with the low-WSS regions in the ascending aorta and the descending aorta. The relationship between oxygen transport and WSS has not yet been determined. As a result, considering WSS or oxygen transport alone is inadequate in investigating atherosclerosis development accurately.

Exercise promotes the blood flow in femoral arteries and contributes to the increase in blood velocity [46]. In the present study, *velocityA* represents the mean blood velocity at rest, *velocityB* represents the mean blood velocity during exercise, and *velocityC* represents the mean blood velocity during steady-state exercise. Following an increment of the velocity at the inlet, the velocity of blood flow in the DLFCA of the residuum increased, the value of WSS increased, and the number of low-WSS regions decreased. The residuum DLFCA with *velocityC* had the lowest rate of atherosclerosis in terms of WSS. The increase in blood velocity decreased the formation rate of atherosclerotic plaque, and thus exercise is beneficial for the prevention and control of atherosclerosis. Moreover, the Sherwood number with *velocityC* was the largest, and the increment of inlet velocity contributed to the increase in Sherwood number in the vascular wall. Thus, the number and area of hypoxia zones in the residuum DLFCA reduced with an increase in inlet velocity. An increase in blood velocity can enhance the oxygen transport in the residuum DLFCA, reducing the number of hypoxia zones. In summary, exercise promotes blood flow and oxygen transport in the residuum, and contributes to the decrease in the rate of atherosclerosis in the DLFCA, based on consideration of WSS and hypoxia.

5. Conclusion

In order to investigate the blood flow and oxygen transport in the residuum DLFCA after amputation, computational models of DLFCAs in both the residuum and the sound contralateral limb were employed. In terms of WSS, the rate of atherosclerosis in the residuum is lower than that of the sound limb after amputation. However, the rate of atherosclerosis in the sound limb is lower than that of the residuum in terms of hypoxia. As a consequence, joint consideration of oxygen transport and WSS is beneficial for investigating atherosclerosis development in the arteries of the lower limb after amputation.

Oxygen transport and blood flow in the residuum DLFCA were simulated numerically in terms of three inlet velocities in order to understand the impact of exercise on the status of the vessel. Exercise is beneficial for oxygen transport by increasing the oxygen flux to the arterial wall, and is helpful in the prevention and control of atherosclerosis in the arteries of the residuum.

This numerical study has some limitations. Firstly, only one case of the residuum and sound limb was employed for the geometric reconstruction; more cases are required for simulating the blood flow and oxygen transport more precisely. Secondly, the assumption of steady flow was applied in this study. The pulsatile flow in vessels could affect the accuracy of WSS values and the Sherwood number. Thirdly, the elasticity of the vascular wall was neglected since it should have little effect on the distribution of blood flow and oxygen tension in this computational simulation. The distribution of oxygen tension and blood velocity was found qualitatively in this study, and it reveals that the investigation of oxygen transport in the residuum vasculature is valuable in understanding the health status of the residuum after amputation.

ACKNOWLEDGMENTS

This work was supported by Grants-in-Aid from the National Natural Science Foundation of China (No. 11272224) and the Project of Sichuan Province Academic and Technical Leaders Cultivate Funding (No. 2012DTPY021).

CONFLICT OF INTEREST

The authors declare that they have no conflicts of interest.

REFERENCES

1. Luo, Y. Z., & Sun, W. (2009). The development of Chinese prostheses since the founding. *Orthopaedic Journal of China*, *17*(17), 1325-1328.

2. Zhao, M. G., Zhang, Y. D., Zhang, Z. J., Liu, W. D., & Peng J. (2008). Characteristics and staged rescue of severe cases in "5.12" Wenchuan megaseism. *China Journal of Modern Medicine*, *18*(16), 2287-2294.

3. Lyon, C. C., Kulkarni, J., Zimersonc, E., Van Ross, E., & Beck, M. H. (2000). Skin disorders in amputees. *Journal of the American Academy of Dermatology, 42*(3), 501-507.

4. Sanders, J. E., Garbini, J. L., Leschen, J. M., Allen, M. S., & Jorgensen, J. E. (1997). A bidirectional load applicator for the investigation of skin response to mechanical stress. *Biomedical Engineering, IEEE Transactions on, 44*(4), 290-296.

5. Portnoy, S., Siev-Ner, I., Shabshin, N., Kristal, A., Yizhar, Z., & Gefen, A. (2009). Patient-specific

analyses of deep tissue loads post transtibial amputation in residual limbs of multiple prosthetic users. *J Biomech, 42*(16), 2686-2693, doi:10.1016/j.jbiomech.2009.08.019.

6. Fraisse, N., Martinet, N., Kpadonou, T. J., Paysant, J., Blum, A., & Andre, J. M. (2008). [Muscles of the below-knee amputees]. *Ann Readapt Med Phys, 51*(3), 218-227, doi:10.1016/j.annrmp.2008.01.012.
7. Schmalz, T., Blumentritt, S., & Reimers, C. (2001). Selective thigh muscle atrophy in trans-tibial amputees: an ultrasonographic study. *Archives of orthopaedic and trauma surgery, 121*(6), 307-312.
8. Lee, W. C., Zhang, M., Jia, X., & Cheung, J. (2004). Finite element modeling of the contact interface between trans-tibial residual limb and prosthetic socket. *Medical engineering & physics, 26*(8), 655-662.
9. Mak, A. F. T., Zhang, M., & Boone, D. A. (2001). State-of-the-art research in lower-limb prosthetic biomechanics-socket interface: A review. *Journal of Rehabilitation Research & Development, 38*(2), 161-173.
10. Renström, P., Grimby, G., Morelli, B., & Palmertz, B. (1982). Thigh muscle atrophy in below-knee amputees. *Scandinavian journal of rehabilitation medicine. Supplement, 9*, 150-162.
11. Dillingham, T. R., Pezzin, L. E., & Shore, A. D. (2005). Reamputation, mortality, and health care costs among persons with dysvascular lower-limb amputations. *Arch Phys Med Rehabil, 86*(3), 480-486.
12. Gudmundsson, G., Matthiasson, S. E., Arason, H., Johannsson, H., Runarsson, F., Bjarnason, H., Helgadottir, K., Thorisdottir, S., Ingadottir, G., Lindpaintner, K., Sainz, J., Gudnason, V., Frigge, M. L., Kong, A., Gulcher, J. R., & Stefansson K. (2002). Localization of a gene for

peripheral arterial occlusive disease to chromosome 1p31. *Am J Hum Genet, 70*(3), 586-592, doi:10.1086/339251.

13. Erikson, U., & Hulth, A. (1962). Circulation of amputation stumps. Arteriographic and skin temperature studies. *Acta Orthop Scand, 32*, 159-170.

14. Qiu, Y., & Tarbell, J. M. (2000). Numerical simulation of oxygen mass transfer in a compliant curved tube model of a coronary artery. *Annals of biomedical engineering, 28*(1), 26-38.

15. Liu, X., Fan, Y., & Deng, X. (2010). Effect of spiral flow on the transport of oxygen in the aorta: a numerical study. *Annals of biomedical engineering, 38*(3), 917-926.

16. Coppola, G., & Caro, C. (2008). Oxygen mass transfer in a model three-dimensional artery. *Journal of The Royal Society Interface, 5*(26), 1067-1075.

17. Tada, S., & Tarbell, J. M. (2006). Oxygen mass transport in a compliant carotid bifurcation model. *Annals of biomedical engineering, 34*(9), 1389-1399.

18. Bateman, R. M., Sharpe, M. D., & Ellis, C. G. (2003). Bench-to-bedside review: microvascular dysfunction in sepsis–hemodynamics, oxygen transport, and nitric oxide. *Critical Care, 7*(5), 359.

19. Wu, S. P., Ringgaard, S., Oyre, S., Hansen, M. S., Rasmus, S., & Pedersen, E. M. (2004). Wall shear rates differ between the normal carotid, femoral, and brachial arteries: An in vivo MRI study. *Journal of Magnetic Resonance Imaging, 19*(2), 188-193, doi:10.1002/jmri.10441.

20. Papaharilaou, Y., Aristokleous, N., Seimenis, I., Khozeymeh, M. I., Georgiou, G. C., Brott, B. C., Eracleous, E., & Anayiotos, A. S. (2013). Effect of head posture on the healthy human carotid bifurcation hemodynamics. *Med Biol Eng Comput, 51*(1-2), 207-218, doi:10.1007/s11517-012-0985-6.

21. Caro, C., Fitz-Gerald, J., & Schroter, R. (1971). Atheroma and arterial wall shear observation, correlation and proposal of a shear dependent mass transfer mechanism for atherogenesis. *Proceedings of the Royal Society of London B: Biological Sciences, 177*(1046), 109-133.

22. Palumbo, R., Gaetano, C., Antonini, A., Pompilio, G., Bracco, E., Ronnstrand, L., Heldin, C. H., & Capogrossi, M. C. (2002). Different effects of high and low shear stress on platelet-derived growth factor isoform release by endothelial cells: consequences for smooth muscle cell migration. *Arterioscler Thromb Vasc Biol, 22*(3), 405-411.

23. Chatzizisis, Y. S., Baker, A. B., Sukhova, G. K., Koskinas, K. C., Papafaklis, M. I., Beigel, R., Jonas, M., Coskun, A. U., Stone, B. V., Maynard, C., Shi, G., Libby, P., Feldman, C. L., Edelman, E. R., & Stone, P. H. (2011). Augmented expression and activity of extracellular matrix-degrading enzymes in regions of low endothelial shear stress colocalize with coronary atheromata with thin fibrous caps in pigs. *Circulation, 123*(6), 621-630.

24. Siogkas, P., Sakellarios, A., Exarchos, T. P., Athanasiou, L., Karvounis, E., Stefanou, K., Fotiou, E., Fotiadis D. I., Naka K. K., Michalis L. K., Filipovic N., & Parodi O. (2011). Multiscale-patient-specific artery and atherogenesis models. *Biomedical Engineering, IEEE Transactions on, 58*(12), 3464-3468.

25. Dowd, G. S. (1987). Predicting stump healing following amputation for peripheral vascular disease using the transcutaneous oxygen monitor. *Annals of the Royal College of Surgeons of England, 69*(1), 31.

26. Holstein, P., Sager, P., & Lassen, N. A. (1979). Wound Healing in Below-Knee Amputations in Relation to Skin Perfusion Pressure. *Acta Orthopaedica, 50*(1), 49-58, doi:10.3109/17453677909024089.

27. Ratliff, D. A., Clyne, C. A. C., Chant, A. D. B., & Webster, J. H. H. (1984). Prediction of amputation wound healing: The role of transcutaneous pO 2 assessment. *British Journal of Surgery, 71*(3), 219-222, doi:10.1002/bjs.1800710320.

28. Caron, M.-A., Thériault, M.-E., Paré, M.-È., Maltais, F., & Debigaré, R. (2009). Hypoxia alters contractile protein homeostasis in L6 myotubes. *FEBS letters, 583*(9), 1528-1534.

29. Dong, R., Jiang, W., Zhang, M., Leung, A., & Wong, M. (2015). Review: Hemodynamic studies for lower limb amputation and rehabilitation. *Journal of Mechanics in Medicine and Biology, 15*(04), 1530005.

30. Standring, S., Ellis, H., Healy, J., Jhonson, D., Williams, A., & Collins, P. (2005). Gray's anatomy: the anatomical basis of clinical practice. *American Journal of Neuroradiology, 26*(10), 2703.

31. Halvorson, E. G., Taylor, H. O. B., & Orgill, D. P. (2008). Patency of the descending branch of the lateral circumflex femoral artery in patients with vascular disease. *Plast. Reconstr. Surg., 121*(1), 121-129, doi:10.1097/01.prs.0000293862.68476.97.

32. Xu, D. C., Zhong, S. Z., Kong, J. M., Wang, G. Y., Liu, M. Z., Luo, L. S., & Gao, J. H. (1988). Applied anatomy of the anterolateral femoral flap. *Plastic and reconstructive surgery, 82*(2), 305.

33. Ku, D. N. (1997). Blood flow in arteries. *Annual Review of Fluid Mechanics, 29*(1), 399-434.

34. Friedman, M., Bargeron, C., Hutchins, G., Mark, F., & Duncan, D. (1992). Effects of arterial compliance and non-Newtonian rheology on correlations between intimal thickness and wall shear. *Journal of biomechanical engineering, 114*(3), 317-320.

35. Moore, J., Maier, S. E., Ku, D. N., & Boesiger, P. (1994). Hemodynamics in the abdominal aorta: a comparison of in vitro and in vivo measurements. *Journal of Applied Physiology, 76*(4),

1520-1527.

36. Caro, C. G., Pedley, T., Schroter, R., Seed, W., & Parker, K. (1978). *The mechanics of the circulation* (Vol. 527): Oxford University Press Oxford.

37. Politis, A. K., Stavropoulos, G. P., Christolis, M. N., Panagopoulos, F. G., Vlachos, N. S., & Markatos, N. C. (2007). Numerical modeling of simulated blood flow in idealized composite arterial coronary grafts: Steady state simulations. *Journal of Biomechanics, 40*(5), 1125-1136, doi:10.1016/j.jbiomech.2006.05.008.

38. Ko, T. H., Ting, K., & Yeh, H. C. (2007). Numerical investigation on flow fields in partially stenosed artery with complete bypass graft: An in vitro study. *International Communications in Heat and Mass Transfer, 34*(6), 713-727, doi:10.1016/j.jcheatmasstransfer.2007.03.010.

39. Ojha, M., Ethier, C. R., Johnston, K. W., & Cobbold, R. S. (1990). Steady and pulsatile flow fields in an end-to-side arterial anastomosis model. *J Vasc Surg, 12*(6), 747-753, doi:10.1067/mva.1990.24365.

40. Kim, Y. H., Kim, J. E., Ito, Y., Shih, A. M., Brott, B., & Anayiotos, A. (2008). Hemodynamic analysis of a compliant femoral artery bifurcation model using a fluid structure interaction framework. *Annals of biomedical engineering, 36*(11), 1753-1763, doi:10.1007/s10439-008-9558-0.

41. Wentzel, J. J., Krams, R., Schuurbiers, J. C., Oomen, J. A., Kloet, J., van der Giessen, W. J., Serruys, P. W., & Slager, C. J. (2001). Relationship between neointimal thickness and shear stress after Wallstent implantation in human coronary arteries. *Circulation, 103*(13), 1740-1745.

42. Batra, R., & Jena, B. (1991). Flow of a Casson fluid in a slightly curved tube. *International journal of engineering science, 29*(10), 1245-1258.

43. Johnston, B. M., Johnston, P. R., Corney, S., & Kilpatrick, D. (2006). Non-Newtonian blood flow in human right coronary arteries: transient simulations. *Journal of Biomechanics, 39*(6), 1116-1128.

44. Chen, J., & Lu, X.-Y. (2006). Numerical investigation of the non-Newtonian pulsatile blood flow in a bifurcation model with a non-planar branch. *Journal of Biomechanics, 39*(5), 818-832.

45. Fan, Y., Jiang, W., Zou, Y., Li, J., Chen, J., & Deng, X. (2009). Numerical simulation of pulsatile non-Newtonian flow in the carotid artery bifurcation. *Acta Mechanica Sinica, 25*(2), 249-255.

46. Shoemaker, J. K., Phillips, S. M., Green, H. J., & Hughson, R. L. (1996). Faster femoral artery blood velocity kinetics at the onset of exercise following short-term training. *Cardiovasc Res, 31*(2), 278-286.

47. Plowman, S. A., & Smith, D. L. (2013). *Exercise physiology for health fitness and performance*: Lippincott Williams & Wilkins.

48. Fournier, R. L. (2011). *Basic transport phenomena in biomedical engineering*: CRC Press.

49. Moore, J., & Ethier, C. (1997). Oxygen mass transfer calculations in large arteries. *Journal of biomechanical engineering, 119*(4), 469-475.

50. Buerk, D. G., & Goldstick, T. K. (1982). Arterial wall oxygen consumption rate varies spatially. *American Journal of Physiology-Heart and Circulatory Physiology, 243*(6), H948-H958.

51. Tarbell, J. M. (2003). Mass transport in arteries and the localization of atherosclerosis. *Annual review of biomedical engineering, 5*(1), 79-118.

52. Okamoto, R., Hatani, M., Tsukitani, M., Suehiro, A., Fujino, M., Imai, N., Takano, S., Watanabe, Y., & Fukuzaki, H. (1983). The effect of oxygen on the development of atherosclerosis in WHHL rabbits. *Atherosclerosis, 47*(1), 47-53.

53. Kolandavel, M. K., Fruend, E. T., Ringgaard, S., & Walker, P. G. (2006). The effects of time varying curvature on species transport in coronary arteries. *Ann. Biomed. Eng., 34*(12), 1820-1832, doi:10.1007/s10439-006-9188-3.

54. Schneiderman, G., Mockros, L. F., & Goldstick, T. K. (1982). Effect of pulsatility on oxygen transport to the human arterial wall. *Journal of Biomechanics, 15*(11), 849-858, doi:10.1016/0021-9290(82)90050-1.

55. Ma, P. P., Li, X. M., & Ku, D. N. (1994). Heat and mass-transfer in separated flow region for high prandtl and schmidt numbers under pulsatile conditions. *Int. J. Heat Mass Transf., 37*(17), 2723-2736.

56. Olgac, U., Kurtcuoglu, V., Saur, S. C., & Poulikakos, D. (2008). Identification of atherosclerotic lesion-prone sites through patient-specific simulation of low-density lipoprotein accumulation. In *Medical Image Computing and Computer-Assisted Intervention–MICCAI 2008* (pp. 774-781): Springer.

57. Steinman, D. A. (2004). Image-based computational fluid dynamics: a new paradigm for monitoring hemodynamics and atherosclerosis. *Current Drug Targets-Cardiovascular & Hematological Disorders, 4*(2), 183-197.

58. Taylor, C. A., Hughes, T. J., & Zarins, C. K. (1998). Finite element modeling of three-dimensional pulsatile flow in the abdominal aorta: relevance to atherosclerosis. *Annals of biomedical engineering, 26*(6), 975-987.

59. Ogawa, S., Gerlach, H., Esposito, C., Pasagian-Macaulay, A., Brett, J., & Stern, D. (1990). Hypoxia modulates the barrier and coagulant function of cultured bovine endothelium. Increased monolayer permeability and induction of procoagulant properties. *Journal of Clinical*

Investigation, 85(4), 1090.

60. Matsushita, H., Morishita, R., Nata, T., Aoki, M., Nakagami, H., Taniyama, Y., Yamamoto, K., Higaki, J., Yasufumi, K., & Ogihara, T. (2000). Hypoxia-induced endothelial apoptosis through nuclear factor-κB (NF-κB)–mediated bcl-2 suppression in vivo evidence of the importance of NF-κB in endothelial cell regulation. *Circulation Research, 86*(9), 974-981.

61. Hulten, L. M., & Levin, M. (2009). The role of hypoxia in atherosclerosis. *Current opinion in lipidology, 20*(5), 409-414.

62. Back, L. H., Radbill, J. R., & Crawford, D. W. (1977). Analysis of oxygen transport from pulsatile, viscous blood flow to diseased coronary arteries of man. *Journal of Biomechanics, 10*(11), 763-774.

63. Schneiderman, G., & Goldstick, T. K. (1978). Significance of luminal plasma layer resistance in arterial wall oxygen supply. *Atherosclerosis, 31*(1), 11-20.

64. Stein, T. R., Martin, J. C., & Keller, K. H. (1971). Steady-state oxygen transport through red blood cell suspensions. *Journal of Applied Physiology, 31*(3), 397-402.

FIGURE CAPTIONS

Figure 1. Geometric models of DLFCAs in (a) sound contralateral limb and (b) residuum.

Figure 2. Meshed models of DLFCAs in (a) sound contralateral limb and (b) residuum.

Figure 3. Distribution of blood velocity in DLFCA of (a) sound contralateral limb and (b) residuum. (c) Mean diameter of DLFCAs and (d) mean velocity of blood flow in DLFCAs of residuum and sound limb.

Figure 4. Wall shear stress (WSS) in DLFCAs of (a) sound contralateral limb and (b) residuum.

Figure 5. Sherwood number in DLFCA of (a) sound contralateral limb and (b) residuum. (c) Mean Sherwood number and (d) mean oxygen tension in DLFCAs of residuum and sound limb.

Figure 6. Distribution of blood velocity in residuum DLFCA with (a) *velocityA*, (b) *velocityB*, and (c) *velocityC*. (d) Mean velocity of blood flow in residuum DLFCA for the three inlet velocities. Streamline distribution in region near outlet of residuum DLFCA with (e) *velocityB* and (f) *velocityC*.

Figure 7. Wall shear stress (WSS) in residuum DLFCA with (a) *velocityA*, (b) *velocityB*, and (c) *velocityC*.

Figure 8. Sherwood number in residuum DLFCA with (a) *velocityA*, (b) *velocityB*, and (c) *velocityC*. (d) Mean Sherwood number in residuum DLFCA for the three inlet velocities.

TABLE CAPTIONS

Table 1. Parameters used in oxygen transport.

Figures:

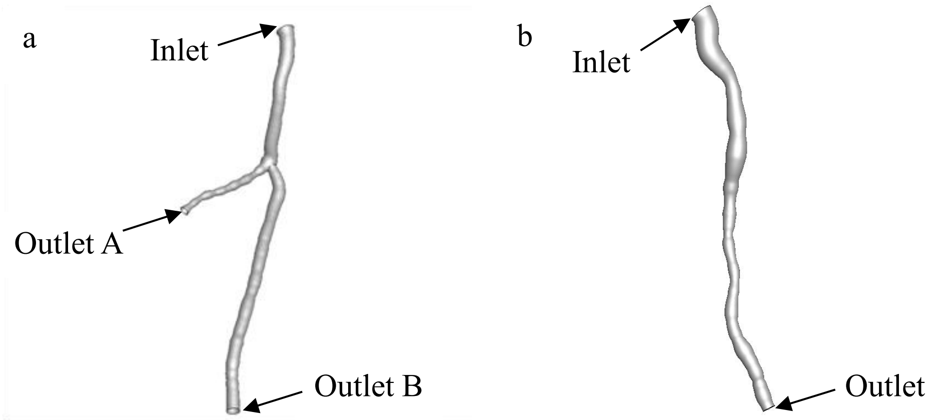

Figure 1. Geometric models of DLFCAs in (a) sound contralateral limb and (b) residuum.

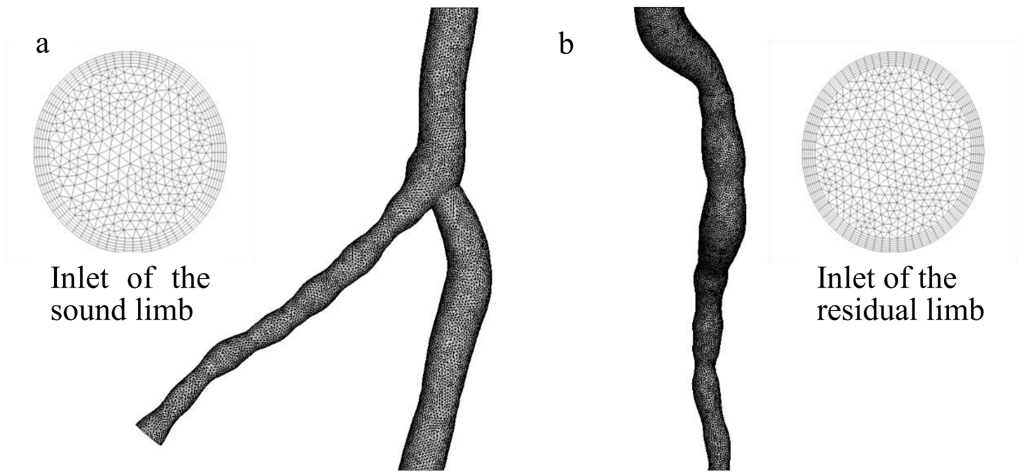

Figure 2. Meshed models of DLFCAs in (a) sound contralateral limb and (b) residuum.

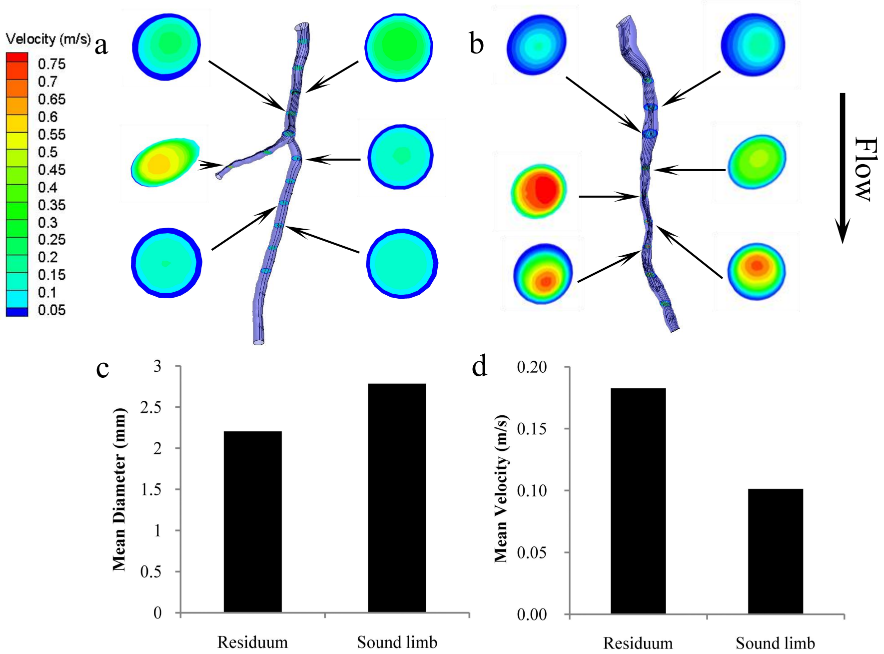

Figure 3. Distribution of blood velocity in DLFCA of (a) sound contralateral limb and (b) residuum. (c) Mean diameter of DLFCAs and (d) mean velocity of blood flow in DLFCAs of residuum and sound limb.

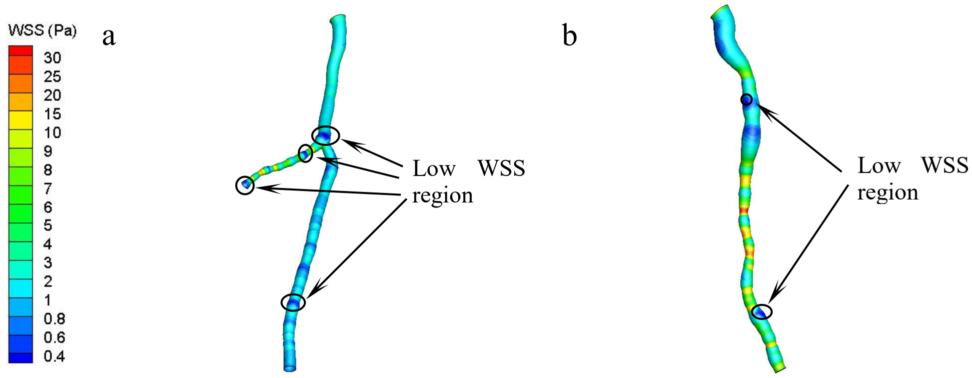

Figure 4. Wall shear stress (WSS) in DLFCAs of (a) sound contralateral limb and (b) residuum.

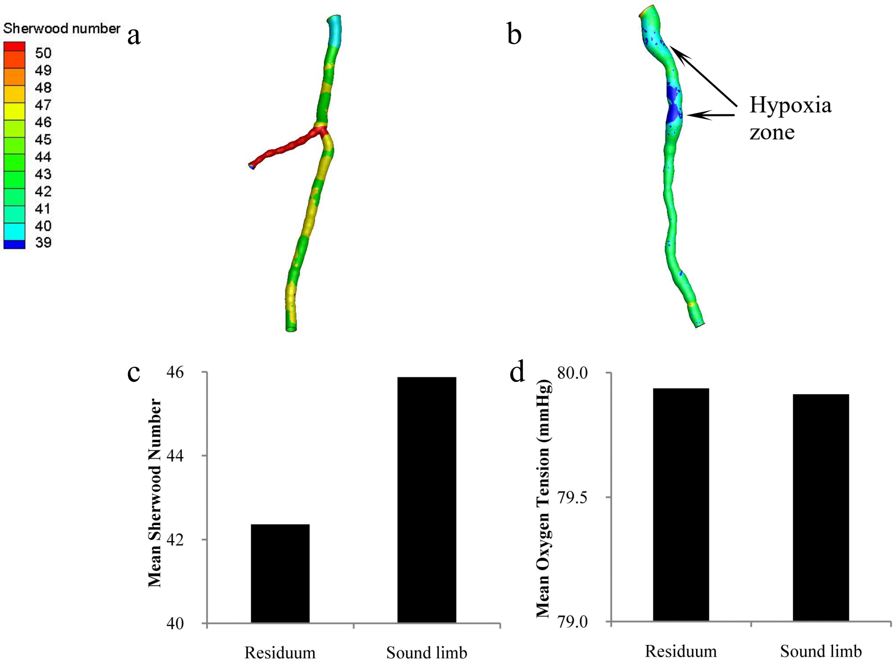

Figure 5. Sherwood number in DLFCA of (a) sound contralateral limb and (b) residuum. (c) Mean Sherwood number and (d) mean oxygen tension in DLFCAs of residuum and sound limb.

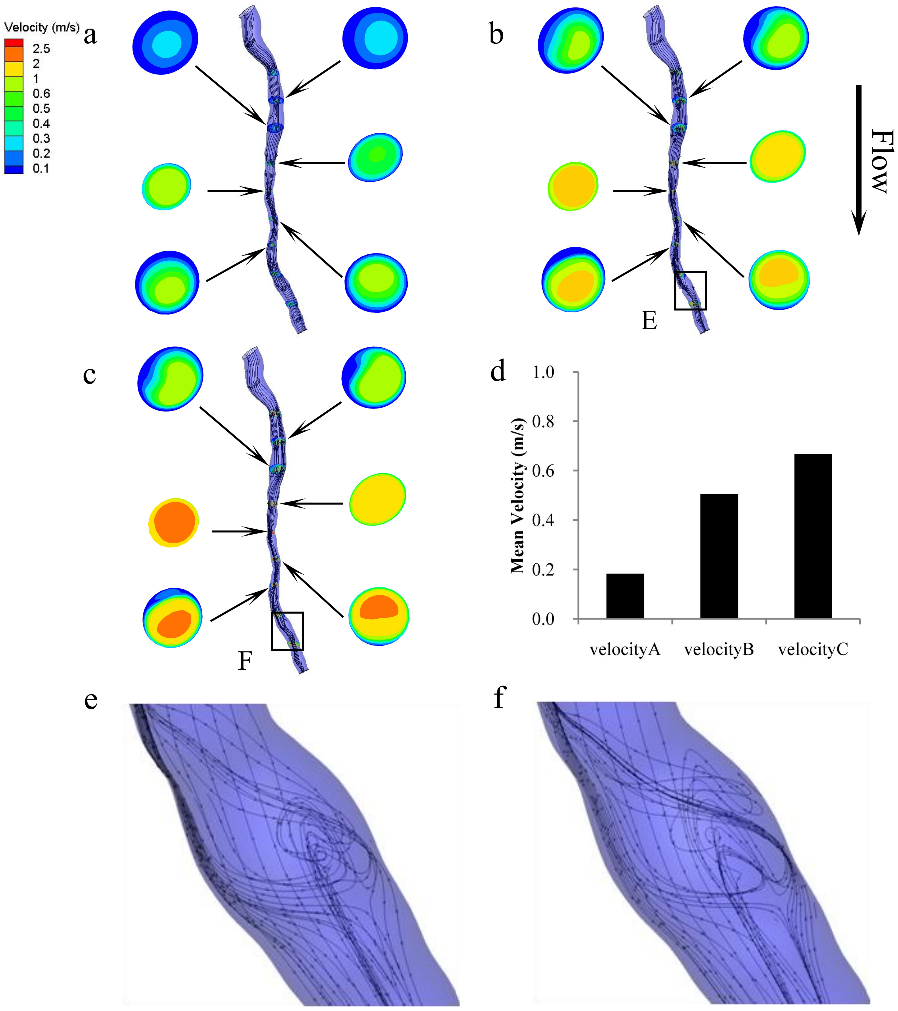

Figure 6. Distribution of blood velocity in residuum DLFCA with (a) *velocityA*, (b) *velocityB*, and (c) *velocityC*. (d) Mean velocity of blood flow in residuum DLFCA for the three inlet velocities. Streamline distribution in region near outlet of residuum DLFCA with (e) *velocityB* and (f) *velocityC*.

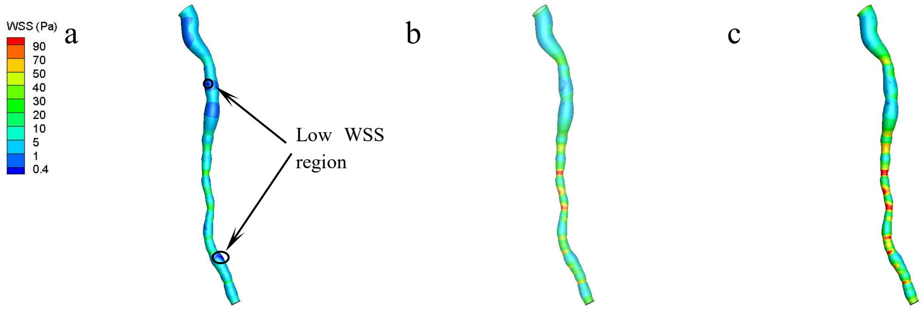

Figure 7. Wall shear stress (WSS) in residuum DLFCA with (a) *velocityA*, (b) *velocityB*, and (c) *velocityC*.

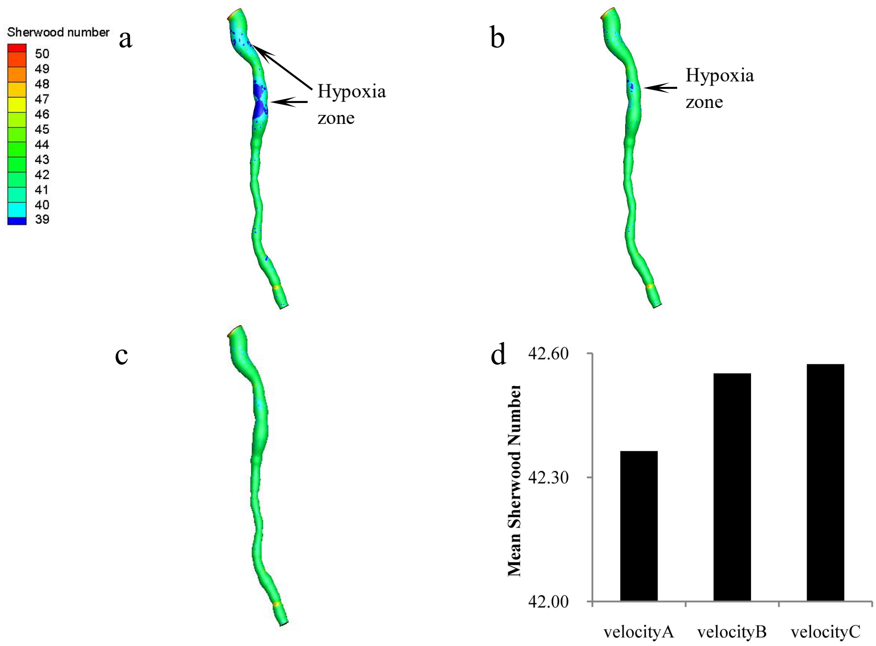

Figure 8. Sherwood number in residuum DLFCA with (a) *velocityA*, (b) *velocityB*, and (c) *velocityC*. (d) Mean Sherwood number in residuum DLFCA for the three inlet velocities.

Tables:

Table 1. Parameters used in oxygen transport.

Parameter	**Value**	**Source**
$[Hb]$	0.2 ml O_2/ml blood	[62]
α	2.5×10^{-5} ml O_2/ml blood/mmHg	[63]
D_b	1.2×10^{-9} m^2/s	[64]
D_c	1.5×10^{-11} m^2/s	[36]
n	2.7	[49]
PO_{50}	26.6 mmHg	[49]